E213: Analysis Of Z^0 Decays

Kanhaiya Gupta and Chelsea Maria John
Supervised by Omer Ogul Oncel

Rheinische Friedrich-Wilhelms Universität Bonn.
Adavnced Lab Course

March 27, 2020

Contents

1 Introduction

The analysis of the Z-boson experiment is designed to give us a first impression on the experiments and methods of analysis in modern particle physics. During this experiment you will analyse data obtained from e^+e^- collisions with the OPAL (Omni-Purpose Apparatus for LEP) detector at the LEP (Large Electron-Positron Collider) storage ring. The experiment E213 consists of two main tasks. In the first part single events are analyzed in detail based on graphical event displays, in order to learn how to associate them with certain processes. In the second part a more quantitative approach is applied and events are analyzed using statistical techniques on Monte Carlo generated samples and hence used to identify particles in real data. This helps us to determine the resonant parameters of Z^0 boson(mass, width), cross sections for different decay channels at different energy levels , lepton universality , number of light neutrino families and Weinberg angle, which can be measured from the forward-backward asymmetry in the reaction $e^+e^- \to \mu^+\mu^-$.

2 Theoretical Background

2.1 Standard Model

The Standard model is used to describe the interactions of fundamental particles in particle physics by means of quantum field theories that are based on the principle of local gauge invariance. The fundamental particles are divided based on their spins into fermions (half–integer spins) and bosons (integer spins). The fermions (quarks, leptons and neutrinos) are building blocks of matters while bosons are mediators of the three fundamental interactions – Electromagnetic (via photons), Strong (via gluons) and Weak (charged current via $W^\pm$ and neutral current via Z^0). The quarks and leptons have three generations where the generations increase in mass and higher generations decay into lower generation particles. Furthermore, each particle has a corresponding anti-particle with opposite charges. Gravity despite being a fundamental force is too weak to play any significant role in particle physics scale. The Standard model also includes the Higgs boson, which is used to give mass to elementary particles.

2.2 Electroweak Unification

The Z^0 boson and photon both carry neutral current and the symmetry group introduced for this electroweak interaction is SU(2)× U(1). This leads to four generators: W^+, W^-, W^0 and Y^0(or B), and acts on left-handed fermion doublets $(e^-\nu_e)(\mu^-\nu_\mu)$ $(\tau^-\nu_\tau)$ (u d) (s c)(b t).
The theoretical gauge particles are identical with observable states only in the case of charged $W^\pm$ bosons. Therefore, it would be assumed that the Y^0 is identical with photon which implies that it couples to neutrinos which doesn't occur in nature. As a result the photon field (A) is described as a quantum mechanical mixture of the W^0 and Y^0 fields. The mixing angle is called Weinberg angle, θ_W and it describes the rotation between the two states of W^0 and Y^0 . In this experiment, it is measured by the forward-backward asymmetry of the $Z^0 \to \mu^+\mu^-$ channel.

$$\begin{pmatrix} Z^0 \\ A \end{pmatrix} = \begin{pmatrix} \cos\theta_W & -\sin\theta_W \\ \sin\theta_W & \cos\theta_W \end{pmatrix} \cdot \begin{pmatrix} W^0 \\ Y^0 \end{pmatrix} \tag{1}$$

2.3 Electron-Positron Interactions

The following e^+e^- interactions are of interest in this experiment:
1) Bhabha (elastic)scattering
2) Annihilation of the e^+e^- into a photon or Z^0 boson which decay back to a fermion anti-fermion pair and hadrons
3) Annihilation of e^+e^- into two or three photons
4) Radiative corrections and higher order processes.

At energies close to Z^0 mass, the cross-section for the process $e^+e^- \to f\bar{f}$ is dominated by the exchange of Z^0 .The t-channel contribution in the Bhabha scattering doesn't not occur in $e^+e^- \to f\bar{f}(f\bar{f}$ excludes $e^+e^-)$ as Z^0 can't change flavours. The cross section dependence on the angle θ between incoming and outgoing electron is different for both s and t-channel. For s-channel it is proportional to $(1 + \cos^2\theta)$ and

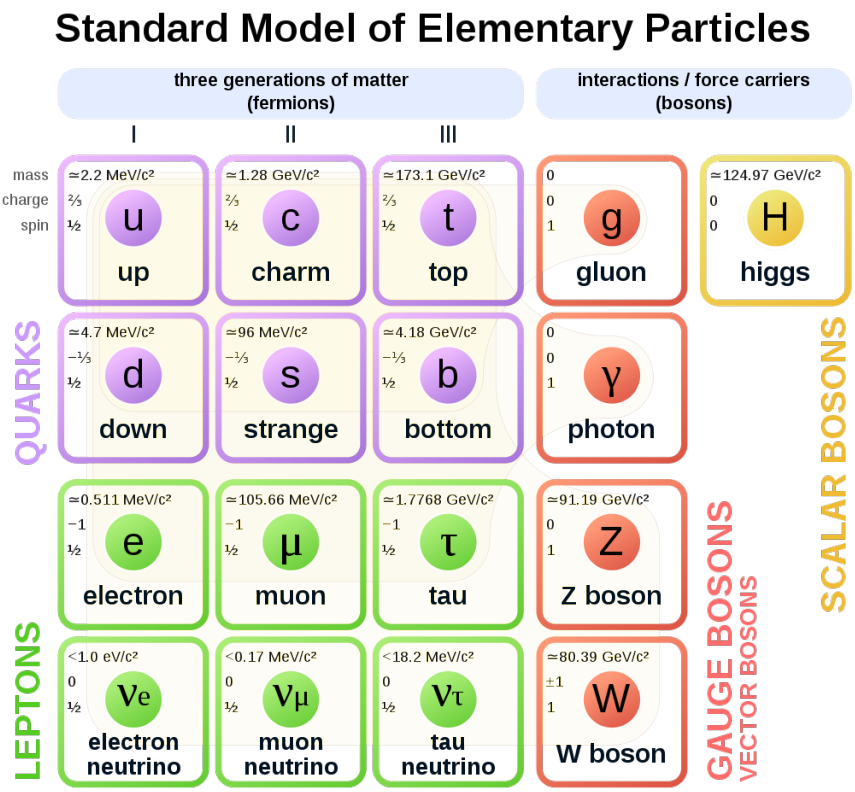

Figure 1: Standard Model[1]

for t-channel $(1-\cos\theta)^{-2}$. Thus, s-channel dominates for large angles while t-channel for small angles. The total decay width of Z^0 is the sum of all the partial decay widths:

$$\Gamma_{Z^0} = \Gamma_e + \Gamma_\mu + \Gamma_\tau + \Gamma_{had} + n_\nu \Gamma_\nu \tag{2}$$

This relation can be used to determine the number of light neutrino generations n_ν.

2.4 Forward Backward Asymmetry

The cross-section at the lowest-order in perturbation theory for the reaction $e^+e^- \to \mu^+\mu^-$ is asymmetric wrt angle θ between the incoming e^- and the outgoing μ^-. This leads to defining a parameter called Forward backward asymmetry (A_{FB}^f) through the cross-section σ in the forward and backward hemispheres

$$A_{FB}^f = \left(\frac{\int_0^1 \frac{d\sigma}{d\cos\theta} d\cos\theta - \int_{-1}^0 \frac{d\sigma}{d\cos\theta} d\cos\theta)}{(\int_0^1 \frac{d\sigma}{d\cos\theta} d\cos\theta + \int_{-1}^0 \frac{d\sigma}{d\cos\theta} d\cos\theta)}\right. \tag{3}$$

At the Z^0 resonance the above equation (3) reduces to

$$A_{FB}^f \approx 3.(1 - 4\sin^2\theta_W)^2 \tag{4}$$

2.5 OPAL Detector

The OPAL detector is a particle detector which is symmetric around the beam pipe (z-axis). It consists of two parts: Tracking detector and Calorimeter. The tracking detector consists of the micro-vertex chamber which is close to the beam pipe, the vertex chamber, the jet chamber and Z-chambers. It is used to detect charged particle tracks and measure the momentum by the curvature of the charged particles in applied magnetic field with semi-conductor detectors and Multi-wire proportional counter. The calorimeter is used to measure the energy deposited by the particles. It contains The ECAL (Electromagnetic calorimeter) and

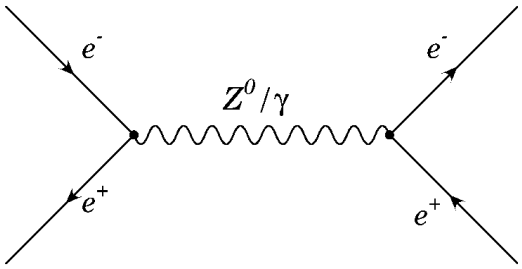

Figure 2: s-channel in Bhabha Scattering of e^+e^- [2]

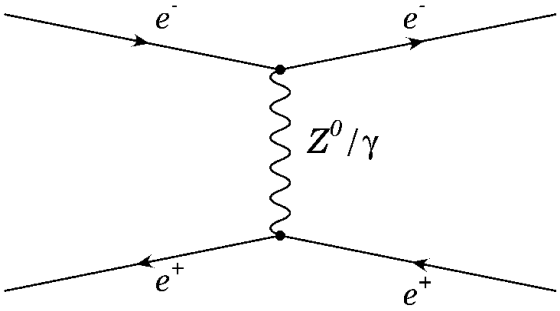

Figure 3: t-channel in Bhabha Scattering of e^+e^-[2]

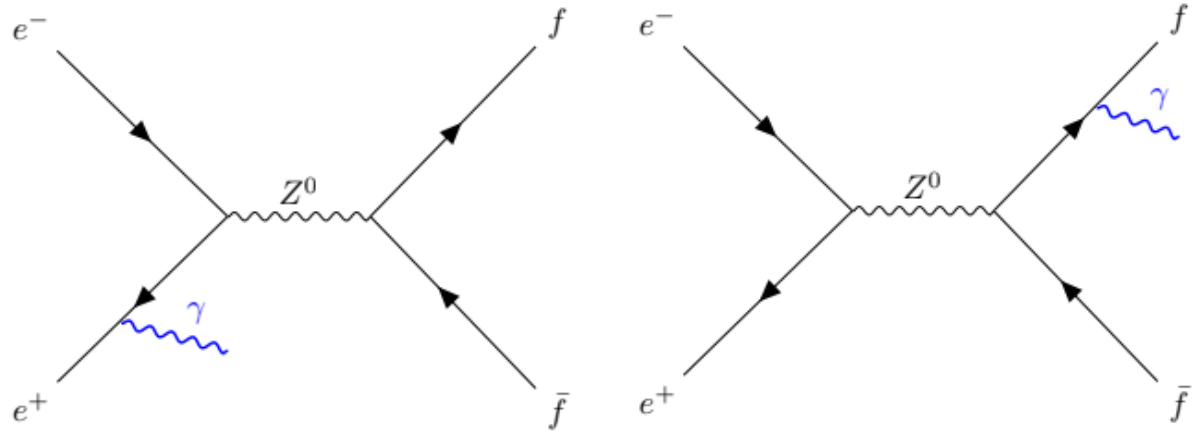

(a) Initial State Radiation (b) Final state radiation

Figure 4: Feynman diagrams for real QED radiative corrections[3].

HCAL (Hadronic calorimeter). Both the calorimeters are built suing alternating planes of heavy matter like steel or copper and detecting planes consisting of scintillation materials. The muons aren't able to deposit much energy in the calorimeter due to its high mass and are detected using muon chambers.

Different particle interact differently with each component of the detector, which allows for the definition of several discriminating variables. The interactions of particles are visualized in the Figure (6). Solid lines in the tracking chamber signify tracks of charged particles, dashed lines signify not found tracks of neutral particles and the bubbles represent the contours of electromagnetic and hadronic showers. Quantitavively, they are explained further in the analysis section of the report .

2.6 Luminosity and Cross-section

The luminosity is a characteristic value of the detector and can be used to determine the cross-section with the event rates known. For a given event rate $\frac{dn}{dt}$, cross-section σ and Luminosity L holds the relation:

$$\frac{dn}{dt} = \sigma.L, n = \sigma \int Ldt \tag{5}$$

3 Part 1:Analysis of Event Displays

The first part is devoted into learning how to distinguish different decay channel by event displays and four discriminating variables. Hence four Monte Carlo simulated with 20 events each are provided. The limited

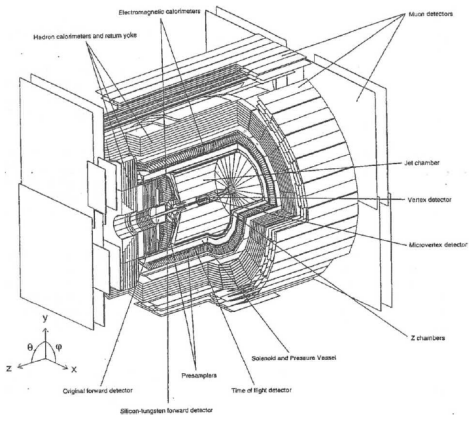

Figure 5: Schematic giagram of the OPAL Detector[3]

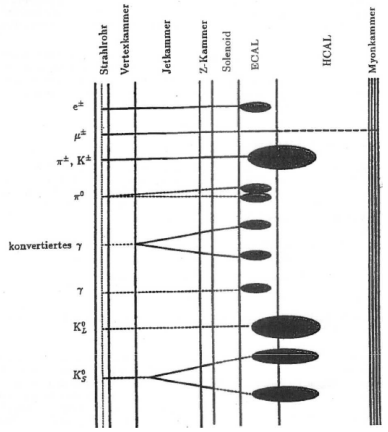

Figure 6: Schematical representation of the signature of elementary particles at the OPAL detector[3].

number of events allows for an example separately. Every sample corresponds to one of the following decay channels:
1) $Z^0 \to e^+e^-$
Being charged particles, they create electromagnetic showers through bremsstrahlung and dissipate their energy in the electromagnetic calorimeter and don't interact with the hadronic calorimeter greatly because of their lepton nature.However, some deviations such as three charged tracks and some showers in the HCAL can be seen and can be attributed to two photon processes that lead to hadronisation or the bremsstrahlung effect.
2) $Z^0 \to \mu^+\mu^-$
Muons are 200 heavier than electrons, they don't initiate showers in either the ECAL nor the HCAL (up to a decent extent) and travel unaffected to the muonchamber where they are detected as two hits on opposite sites.
3)$Z^0 \to \tau^+\tau^-$
Tau particles have a short lifetime and they decay quickly which means we can have deviations from the two charged tracks up to five charged tracks.Tau particles can be identified by their decay product and since they are heavier than electrons and muons, their sum of momentum is less than that of the electrons and muons for the same CMS energy. Since the tau particles decay to charged leptons and mesons, we have showers in the ECAL.
4)$Z^0 \to qq$
Since quarks cannot exist freely and they form jets of hadrons via strong interaction,they have a high number of charged tracks. These hadronic jets contain a wide range of charged/uncharged particles which showers in both the ECAL and HCAL.

The following variables, are measured for each event:

- Ctrk(N): Number of charged tracks
- Ctrk(Sump): Momentum of all charged tracks
- Ecal(SumE): Total energy deposited in the electromagnetic calorimeter
- Hcal(SumE): Total energy deposited in the hadronic calorimeters

The measured values for each events are listed in Tables 9, 10, 11 and 12 in the appendix. In addition to these four variable, it is possible to display each event and the corresponding response of the detector separately using the program GROPE. Figure 7 shows the GROPE output of a typical event from each of the afore mentioned decay channels.

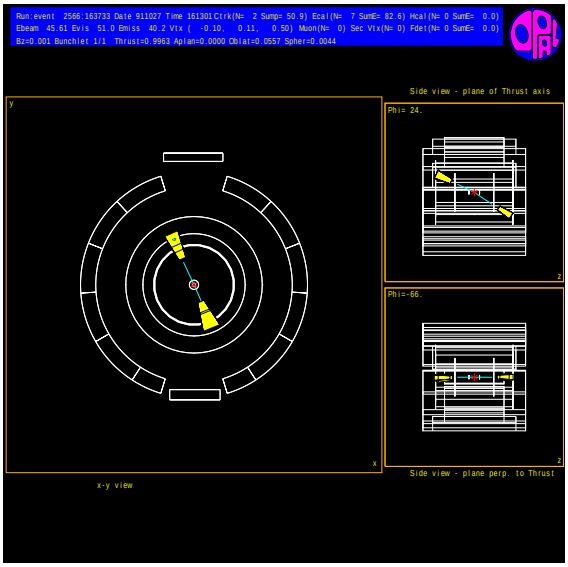

$Z^0 \to e^+e^-$

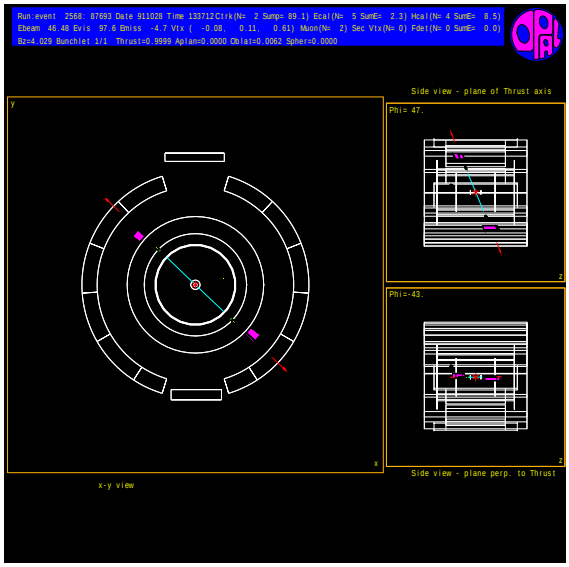

$Z^0 \to \mu^+\mu^-$

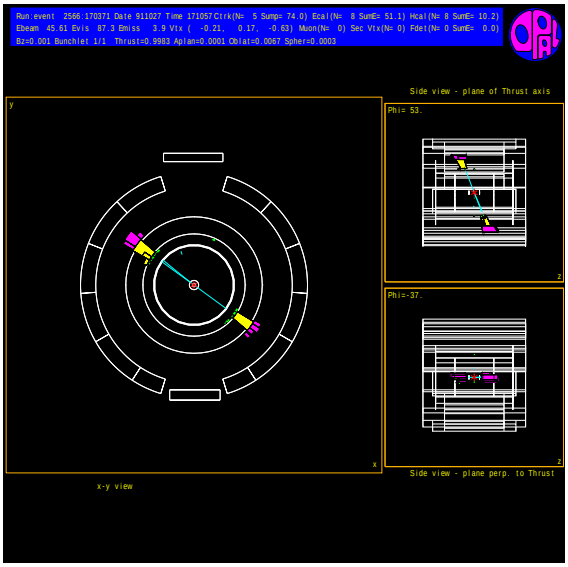

$Z^0 \to \tau^+\tau^-$

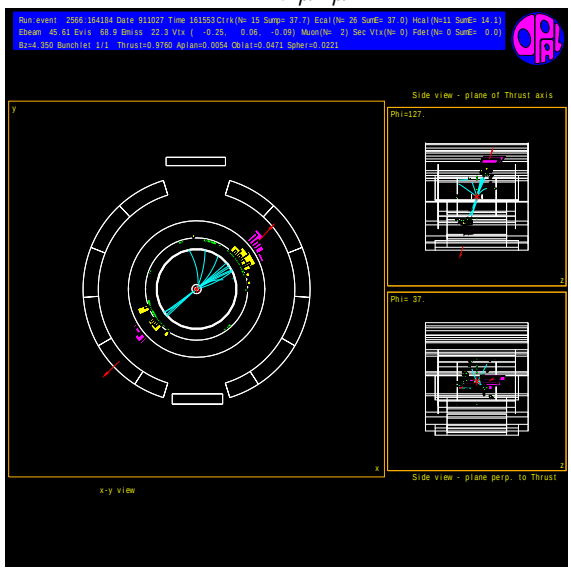

$Z^0 \to hadrons$

Figure 7: Event displays for four different decay modes of e^+e^-[3]

3.1 Determination of appropriate cuts for event classification

Samples usually contain many more than 20 events. It is not feasible to do event classification using event displays for large samples. It is therefore used to choose cuts on the four variables, which theoretically allow a completely electronic classification of events. The cuts are chosen based on a histogram for each of the four variables, which are shown in Figures:(8),(9),(10)(11)

The histogram show, that a clear distinction between hadronic and fermionic decays is possible by setting a cut on the variable Ctrk(N). This is consistent with Figure(7) and expected, the number of charged tracks clearly is largest for the hadronic decay.

Furthermore the decay channel $Z^0 \to e^+e^-$can be separated from the rest by cutting on the variable Ecal(SumE). This is also consistent with Figure(7) and expected, because the electrons/positrons are entirely stopped within the electronic calorimeter.

The only necessary distinction left in this point is the one between $Z^0 \to \mu^+\mu^-$, $Z^0 \to \tau^+\tau^-$. Particles from both decay channels deposit similar amounts of energy in the hadronic calrimeter, which makes the variable Hcal(SumE) inappropriate. However in the $Z^0 \to \tau^+\tau^-$, subsequent decays of $\tau^\pm$ leptons creates

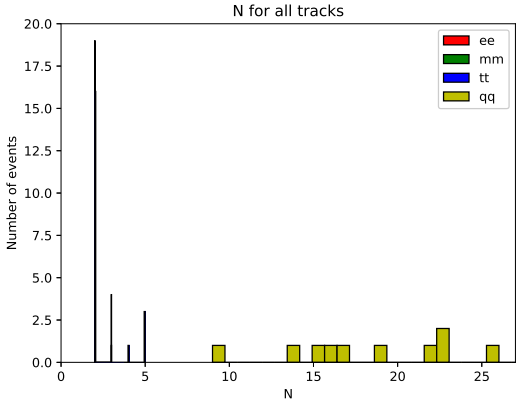

Figure 8: Histogram showing the number of charged tracks

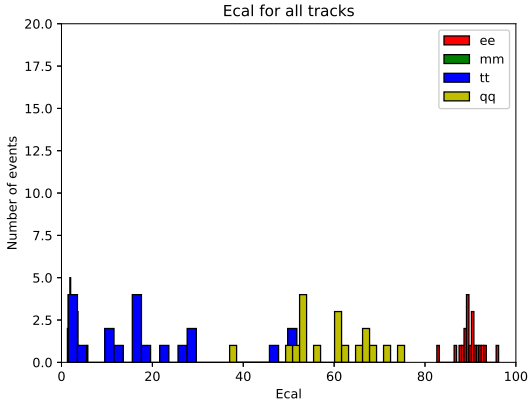

Figure 9: Histogram showing the energy deposited in the Electromagnetic Calorimeter

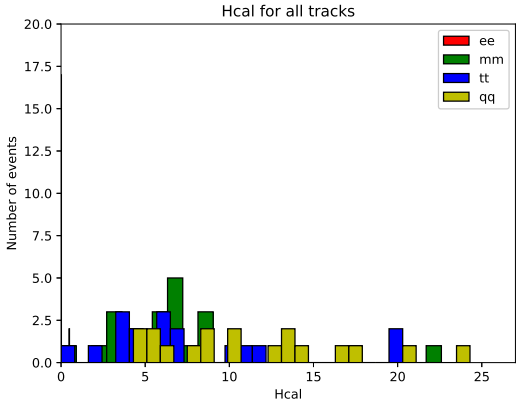

Figure 10: Histogram showing the energy deposited in the Hadronic Calorimeter

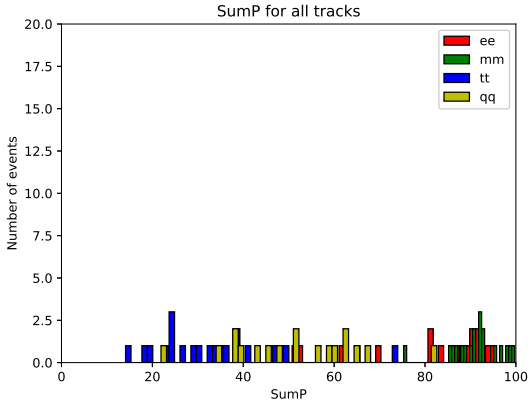

Figure 11: Total scalar sum of track momenta

neutrinos which carry away momentum. Due to invisibility of neutrinos to the detector, the sum of momenta is lower for the $Z^0 \to \tau^+\tau^-$ channel.

Based on the these considerations, we choose the cuts in Figure (12) as a tree like diagram. These cuts can now be applied to test samples, where the true decay channels is not known.

3.2 Event classification for test sample

The cuts from section 3.1 are now used to classify events from the sample TEST1, which is one of the four test samples provided to us. Since, the true decay channels of events from this sample are not known, it is not possible to determine the effectiveness of the cuts for this sample. It is however possible to compare the classification based on cuts with one done by eye based on event displays. Regarding the fact, that these cuts will be redefined in section 4 for the second part of this experiment, this comparison suffices as figure of merit.

The measured values for each variable and the decay channel classification results are given in Table1. The results in this table show, that the applied cuts are mostly consistent with an event display based classification. Hence we take these cuts as a basis for the second part of the experiment.

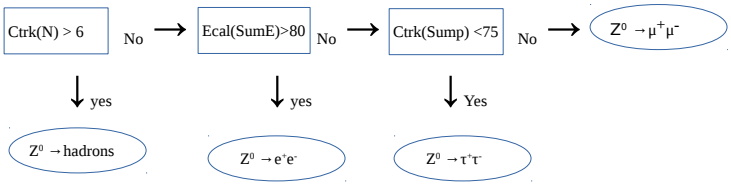

Figure 12: Preliminary Cuts

Table 1: Measured values and classification results for the sample TEST1

Run	Event	Ctrk(N)	Ctrk(SumP)	Ecal(SumE)	Hcal(SumE)	Event display classification	Cut classification
4353	1080	19	39.5	44.3	15.6	$Z^0 \to qq$	$Z^0 \to qq$
4353	2387	36	42.8	57.1	12.5	$Z^0 \to qq$	$Z^0 \to qq$
4353	5386	02	95.7	93.4	0.0	$Z^0 \to e^+e^-$	$Z^0 \to e^+e^-$
4353	6057	02	90.8	1.4	4.1	$Z^0 \to \mu^+\mu^-$	$Z^0 \to \mu^+\mu^-$
4353	6696	04	36.5	35.8	10.8	$Z^0 \to \tau^+\tau^-$	$Z^0 \to \tau^+\tau^-$
4353	7137	02	97.0	2.2	8.9	$Z^0 \to \mu^+\mu^-$	$Z^0 \to \mu^+\mu^-$
4353	7219	68	42.9	48.5	6.2	$Z^0 \to qq$	$Z^0 \to qq$
4353	8323	5	35.0	40.8	3.3	$Z^0 \to \tau^+\tau^-$	$Z^0 \to \tau^+\tau^-$
4353	861	21	75.8	45.8	21.0	$Z^0 \to qq$	$Z^0 \to qq$
4353	9149	02	95.2	1.3	7.9	$Z^0 \to \mu^+\mu^-$	$Z^0 \to \mu^+\mu^-$
4353	9289	2	22.7	34.4	0.0	$Z^0 \to e^+e^-$	$Z^0 \to e^+e^-$
4353	9593	4	44.3	37.8	2.6	$Z^0 \to \tau^+\tau^-$	$Z^0 \to \tau^+\tau^-$
4353	9880	21	53.1	36.2	22.9	$Z^0 \to qq$	$Z^0 \to qq$
4353	10900	2	89.5	92.0	0.0	$Z^0 \to e^+e^-$	$Z^0 \to e^+e^-$
4353	11844	2	89.1	89.7	0.0	$Z^0 \to e^+e^-$	$Z^0 \to e^+e^-$
4353	13556	2	4.1	4.4	0.0	$Z^0 \to e^+e^-$	$Z^0 \to e^+e^-$
4353	14063	2	87.8	1.4	4.3	$Z^0 \to \mu^+\mu^-$	$Z^0 \to \mu^+\mu^-$
4353	14640	2	75.3	90.0	0.0	$Z^0 \to e^+e^-$	$Z^0 \to e^+e^-$
4353	14744	2	93.7	1.6	6.8	$Z^0 \to \mu^+\mu^-$	$Z^0 \to \mu^+\mu^-$
4353	15775	2	67.1	93.6	0.0	$Z^0 \to e^+e^-$	$Z^0 \to e^+e^-$

4 Part 2: Statistical analysis of Z^0 decays

This part is dedicated to the analysis of large data samples. This is required for an appropriate precision in the measurement of the Z parameters (e.g. Z mass and decay width). An analysis is based on event displays is no longer feasible. The software ROOT is used for the statistical analysis. ROOT allows user to set cuts on certain variables and apply to data. Finally the resulting distribution for each variable can be plotted as histogram. The variable available to us are the same as in section-3 with some additions:

- NCHARGED: Number of charged tracks (previously Ctrk(N))
- PCHARGED: Total scalar sum of track momenta in GeV (previously Ctrk(SumP)
- E_ECAL: Total energy deposited in the electromagnetic calorimeter in GeV (previously Ecal(SumE))
- E_HCAL: Total energy deposited in the hadronic calorimeter in GeV (previously Hcal(SumE))
- E_LEP: Energy of the LEP beam in GeV ($\sqrt{s}$)
- COS_THRU: Cosine of the angle between beam axis and thrust axis
- COS_THET: Cosine of the angle between the incoming positron and outgoing positive particle

4.1 Determination of cuts for particle identification

Similar to Part I (section 3), there are four sets of Monte Carlo generated samples available. One for each of the four decay modes described in section3, additionally there is one out of six possible data samples with unknown decay channel. The first data sample was assigned to us for this part of the analysis.

The cuts are also determined in a similar fashion to section3.1. Histograms for each of the variables are plotted and examined. Once a discriminating variable is found, it is plotted in a restricted interval to improve the accuracy of the cut. This process is repeated until each decay channel can be identified. Due to the increase in statistics compared to the analysis in section 3, it is possible to redefine the cuts from each events display.

The distribution of all the variables for each of the Monte carlo are shown in Figures 24, 25, 26, 27. And that of the Pcharged for all the Monte Carlo samples in Figure 28. The figures show that some distributions are non-physical (e.g. peak for COS_THET at 1000). Before any particle identification is done, a set of cuts is applied. Namely Pcharged > 0 and Ncharged > 0. The first cut done because events with no charged tracks in case of charged particle makes no sense. Regardless of any other cuts for particle identification, this set of cuts will always be applied and referred to as pre-selection cuts.

The Final cuts used for particle identification which are based on the histograms is shown in Figure 13, as a tree diagram. The cuts after the classifications as $Z^0 \to e^+e^-$ event is needed to isolate the s-channel. This can be done due to the angular dependence of s-channel and t-channel (section 4.2). Likewise, the cut after classification as $Z^0 \to \mu^+\mu^-$ is needed to remove unphysical events. This is especially important, because the variable COS_THET will be needed to measure the forward backward asymmetry.

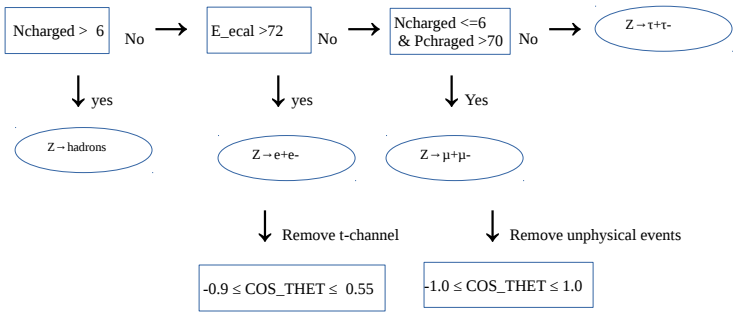

Figure 13: Final Cuts for particle identification

4.2 Efficiency matrix

The determined cuts can now be used on the Monte Carlo generated events. The histograms of the variable by applying the cuts on the Monte Carlo samples are shown in Figures 29, 30, 31, 32. By observing how the samples for each decay mode are classified, it is possible to obtain an efficiency matrix ϵ. It is the measure for the effectiveness of our cuts. In an ideal case, it is diagonal. The efficiency of a process is defined as the ratio of number of events left after a cut, to the total number of events without a cut. For example if a cut i is applied to a process j, the efficiency is given by $\epsilon_{ij} = \frac{N_i}{N_j}$.An efficiency matrix can be defined in the following ways:

$$\epsilon = \begin{pmatrix} \frac{N_{ee}}{N_{ee}} & \frac{N_{ee}}{N_{\mu\mu}} & \frac{N_{ee}}{N_{\tau\tau}} & \cdot & \cdot & \cdot \\ \frac{N_{\mu\mu}}{N_{ee}} & \frac{N_{\mu\mu}}{N_{\mu\mu}} & \cdot & \cdot & & \\ \frac{N_{\tau\tau}}{N_{ee}} & & & \cdot & \cdot & \\ & & & & & \end{pmatrix} \tag{6}$$

Let N_{obs} be the vector with the observed number of events for each decay channel. N_{phy} be the vector with the actual physical number of events for each decay channel and ϵ_{ij} be the efficiency matrix. Then

$$N_{obs} = \epsilon_{ij}.N_{phy} \implies N_{phy} = \epsilon_{ij}^{-1}.N_{obs} \tag{7}$$

The matrix can be obtained from the values given in Table 2. It shows that resulting number of events classified belong to the respective decay channel after applying the cuts from section 4.1.

Table 2: Table

Monte Carlo Sample	No of events classified as				No of events in sample
	$Z^0 \to e^+e^-$	$Z^0 \to \mu^+\mu^-$	$Z^0 \to \tau^+\tau^-$	$Z^0 \to had$	
Electron sample	21425	1	203	0	32677
Muon sample	0	82395	173	0	85984
Tauon sample	408	2502	74597	481	78826
Hadron sample	25	0	976	98043	98563

It should be noted that the number of electrons from the Monte Carlo sample is too low, because of the cut to isolate the s-channel contribution. Hence, using the s-channel distribution ($1 + \cos^2\theta$), their number in the s-channel has to be corrected by the factor given in equation(8). In order to filter out the t-channel events , we are looking for the events $\cos\theta < 0.55$ and $\cos\theta >$ -0.9, since the t-channel contributins are due to the elastic scattering the one, very close to the beam axis. This gives the total number of events in the s-channel. The differential cross-section for both s and t-channel is shown in Figure 23. We clearly, see that the contribution from the t-channel is dominated for $cos\theta > 0.55 \quad \& \leq 1$. And in reality we need to cut the t-channel domination for $cos\theta < 0.9 \quad \& cos\theta \geq -1$ as shown in Figure 14.

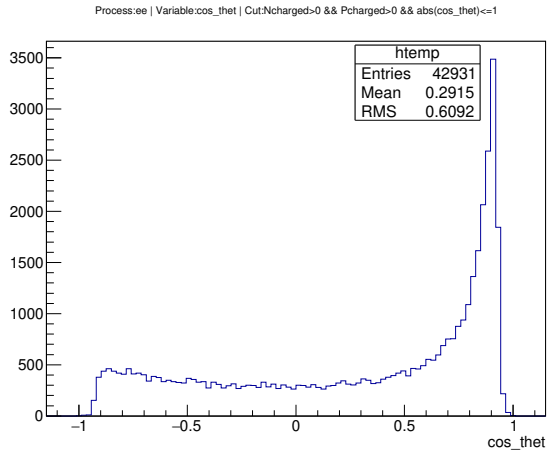

Figure 14: Events for $Z^0 \to e^+e^-$ with both s & t-channel

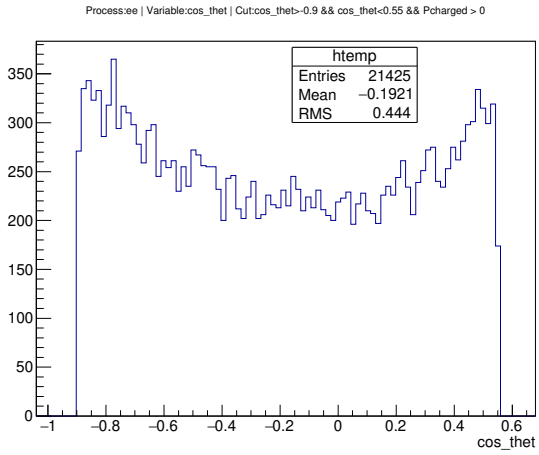

Figure 15: Events for $Z^0 \to e^+e^-$ in s channel after cut

$$\frac{\int_{-1}^{1} 1 + \cos^2\theta d\cos\theta}{\int_{-0.9}^{0.55} 1 + \cos^2\theta d\cos\theta} \approxeq 1.5252 \tag{8}$$

The efficency of the cut is given as

$$\epsilon = \begin{pmatrix} 6.50 \times 10^{-1} & 0 & 5.18 \times 10^{-3} & 2.54 \times 10^{-4} \\ 3.06 \times 10^{-5} & 9.58 \times 10^{-1} & 3.17 \times 10^{-2} & 0 \\ 6.2 \times 10^{-3} & 2.01 \times 10^{-3} & 9.46 \times 10^{-1} & 9.9 \times 10^{-3} \\ 0 & 0 & 6.10 \times 10^{-3} & 9.95 \times 10^{-1} \end{pmatrix} \tag{9}$$

Whether or not an event passes a series of cuts can be seen as a random experiment with two outcomes. The error can thus be estimated by the standard deviation of a binomial distribution.

$$\Delta\epsilon = \sqrt{\frac{\epsilon}{N}.(1-\epsilon)} \tag{10}$$

Where ϵ refers to a single element from ϵ matrix and N to the respective number of total events in Table 2. Using this, the following uncertainties are obtained:

$$\Delta\epsilon = \begin{pmatrix} 2.64\times10^{-3} & 0 & 2.56\times10^{-3} & 5.08\times10^{-4} \\ 3.06\times10^{-5} & 6.84\times10^{-4} & 6.24\times10^{-4} & 0 \\ 4.34\times10^{-4} & 1.53\times10^{-4} & 8.05\times10^{-4} & 3.15\times10^{-4} \\ 0 & 0 & 2.77\times10^{-3} & 2.25\times10^{-1} \end{pmatrix} \tag{11}$$

For the calculation on the data sample, the inverse of the efficiency matrix is needed. The vector N_{phy} is not known for the data sample and thus has to be determined from the inverted efficiency matrix and N_{obs} which is obtained by using the cut from the section 4.1 on the data sample. The python programming language provides a numerical matrix inversion and multiplication within the package numpy. The $\Delta\epsilon^{-1}$ is caluclated as reference[5].

$$(\Delta\epsilon^{-1})^2_{\alpha\beta} = (\epsilon^{-1})^2_{\alpha i}.(\Delta\epsilon)^2_{ij}.(\epsilon^{-1})^2_{j\beta} \tag{12}$$

Hence the following matrices are obtained:

$$\epsilon^{-1} = \begin{pmatrix} 1.540 & 1.760\times10^{-5} & -8.420\times10^{-3} & -3.080\times10^{-4} \\ 2.800\times10^{-4} & 1.040 & -3.490\times10^{-2} & 3.480\times10^{-4} \\ -1.000\times10^{-2} & -2.200\times10^{-3} & 1.057 & -1.050\times10^{-2} \\ 6.000\times10^{-5} & 1.360\times10^{-5} & -6.480\times10^{-3} & 1.006 \end{pmatrix} \tag{13}$$

and

$$\Delta\epsilon^{-1} = \begin{pmatrix} 6.256\times10^{-3} & 2.106\times10^{-6} & 3.747\times10^{\cdot4} & 7.057\times10^{-5} \\ 4.180\times10^{-5} & 7.328\times10^{-4} & 6.316\times10^{-4} & 1.724\times10^{-5} \\ 2.151\times10^{-5} & 1.647\times10^{-4} & 8.842\times10^{-4} & 3.229\times10^{-4} \\ 2.907\times10^{-6} & 1.619\times10^{-6} & 2.873\times10^{-4} & 2.223\times10^{-4} \end{pmatrix} \tag{14}$$

5 Analysis of OPAL Data

5.1 Event Numbers and Cross-section

With the preparatory work done, it is now possible to analyse a set of real OPAL data. We were assigned data1. The events were recorded on different energies. In Figure(17,18,19,20,21), the distribution of the different variable can be seen.

First we want to know the number of events N_{obs} in the different decay channels. To separate the centre of mass energies, we first choose energy intervals. Surprisingly there are not only the discrete energies given in reference[3], but contributions of much different energy. With the chosen intervals all different energies are included.

To analyse the data, the cuts for the different channels (Figure 13) were applied. The received number of events can be seen in Table 3. To obtain the real number N_{phy}, one has to correct the values with the efficiency matrix, which was calculated in section 4.2. The results are can be found in Table 3. The error is calculated with Gaussian error propagation

$$\Delta N_{phy} = \sqrt{(\Delta\epsilon^{-1}.N_{obs})^2 + (\epsilon^{-1}\Delta N_{obs})^2} \tag{15}$$

where $\delta N_{obs} = \sqrt{N_{obs}}$

To calculate the cross-section in the hadronic and leptonic decay channels the relation

$$\sigma = \frac{N_{phy}}{\int Ldt} + C(E_{CMS}) \tag{16}$$

is used. The integrated luninosity $\int Ldt$ error and the radiation correction factor $C(E_{CMS})$ are known from the reference[3]. The error in σ is calculated as

$$\Delta\sigma = \sqrt{\left(\frac{\Delta N_{phy}}{\int Ldt}\right)^2 + \left(\frac{N_{phy}.\Delta\int Ldt}{(\int Ldt)^2}\right)^2} \tag{17}$$

Table 3: Number of recorded events with applied cuts and the number of events corrected by the effciency matrix

E_{CMS}/(GeV)	88.47	89.46	90.22	91.22	91.97	92.96	93.71
N_{obs}							
N_{ee}	632	642	571	4977	764	3767	537
$N_{\mu\mu}$	131	229	320	3678	659	251	308
$N_{\tau\tau}$	199	253	303	4151	697	310	328
N_{qq}	3552	5344	7577	93293	15388	6691	7461
N_{phy}							
N_{ee}	970 ± 38	984±38	874±36	7554±109	1165±42	574±29	821±35
$N_{\mu\mu}$	130 ±11	231±15	325±18	3714±61	666±25	252±15	311±17
$N_{\tau\tau}$	166 ±14	204±15	234±17	3350±72	566±26	262±17	262±18
N_{qq}	3568±59	5369±73	7613±87	93741±307	15461±124	6723±82	7496±86

Table 4: : Calculated cross-sections for all decay channels with equation 16 for different center of mass energies. The error was calculated using equation 17

$E_{CMS}/(GeV)$	88.47	89.46	90.22	91.22	91.97	92.96	93.71
$\sigma_{ee}(nb)$	1.528±0.058	1.834±0.07	2.443±0.089	2.779±0.039	2.045±0.068	1.188±0.063	0.092±0.047
$\sigma_{\mu\mu}(nb)$	0.0284±0.054	0.0466±0.089	1.134±0.043	1.549±0.042	1.263±0.042	0.517±0.034	0.326±0.023
$\sigma_{\tau\tau}(nb)$	0.337±0.066	0.396±0.093	0.918±0.041	1.433±0.077	1.106±0.043	0.5182±0.037	0.262±0.023
$\sigma_{qq}(nb)$	7.287±0.099	14.189±0.161	25.836±0.27	37.724±0.236	28.896±0.288	13.829±0.26	8.177±0.140

5.2 Forward Backward Asymmetry

The forward-backward asymmetry of the muon final states can be investigated by considering the events in forward and backward driection. In our set, this can be done by analyzing the number of events for Nforward and Nbackward for $\cos\theta$ >0 (<0) and $\cos\theta$ <=1 (>=-1) respectively. The forward-backward asymmetry is given by

$$A_{FB}^f = \frac{(\int_0^1 \frac{d\sigma}{d\cos\theta} d\cos\theta - \int_{-1}^0 \frac{d\sigma}{d\cos\theta} d\cos\theta)}{(\int_0^1 \frac{d\sigma}{d\cos\theta} d\cos\theta + \int_{-1}^0 \frac{d\sigma}{d\cos\theta} d\cos\theta)} = \frac{\sigma_F - \sigma_B}{\sigma_F + \sigma_B} + C_{AS} = \frac{N_F - N_B}{N_F + N_B} + C_{AS} \tag{18}$$

with

$$\Delta A_{FB}^f = \sqrt{\left(\frac{N_B.\Delta N_F}{(N_B+N_F)^2}\right)^2 + \left(\frac{N_F.\Delta N_B}{(N_B+N_F)^2}\right)^2} \tag{19}$$

$$A_{FB}^{peak} = 3.(1 - 4\sin^2\theta_W)^2 \tag{20}$$

$$\Delta\sin^2\theta_W = \frac{\Delta A_{FB}^{peak}}{8\sqrt{3.A_{FB}^{peak}}} \tag{21}$$

The radiation correction C_{AS} are given in reference[3]. The resuting values are listed in the Table 5.With the forward-backward asymmetry, it is now possible to calculate the Weinberg angle $\sin^2\theta_W$. Near the Z resonance, it is given by equation (20). The closest value to M_Z is 91.22 GeV, so the Weinberg angle is determined with this value (Table 5). Since the Monte Carlo is also simulated at this energy, $\sin^2\theta_W$ was also calculated for this sample. The result agrees with the literature[3] value of $\sin^2\theta_W$ =0.2312.

Table 5: Forward-backward asymmetry of the muon decay channels calculated by investigating the number of events in forward /backward direction. At $E_{CMS} \approx M_Z$ the Weinberg angle can be determined with equation 20.

$E_{CMS}/(GeV)$	88.47	89.46	90.22	91.22	91.97	92.96	93.71	MonteCarlo
N_F	56	116	138	1820	328	150	171	40587
N_F	75	113	182	1858	331	101	137	41079
A_{FB}	-0.12356	0.0323	-0.12070	0.00796	0.02573	0.2574	0.2042	0.00602
ΔA_{FB}	± 0.043	±0.033	±0.027	±0.0082	±0.0194	±0.031	±0.028	±0.0017
$\sin^2\theta_W$				0.2371				0.2275
				±0.0056				±0.0027

5.3 Lepton Universality

The cross-section of leptons are equal at the Z^0 resonance. To verify that, we have a closer look at the cross-sections at $E_{CMS} = 91.22$ GeV. From Table 4, we get the folowing results:

$$\begin{aligned} \sigma_{ee} &= 2.779 \pm 0.0039 \\ \sigma_{\mu\mu} &= 1.549 \pm 0.042 \\ \sigma_{\tau\tau} &= 1.433 \pm 0.077 \end{aligned} \tag{22}$$

From lepton universality one expects these cross-sections to be same. For the muons and the tauons the deviation is small, nevertheless larger than one sigma deviation. The largest deviation can be found for the electrons cross-section. There could be numerous reasons for the observed deviation.

The electron channels consists of two channels, s and t-channel. Also all considered processes may be subject to statistical fluctuations and systematical errors.

To inspect the lepton universality, further the ratio of the hadronic to the leptonic channel is calculated in the following

$$\begin{aligned} R_{ee} &= \frac{\sigma_{qq}}{\sigma_{ee}} \quad = 13.575 \pm 0.084 \\ R_{\mu\mu} &= \frac{\sigma_{qq}}{\sigma_{\mu\mu}} \quad = 24.354 \pm 0.1859 \\ R_{\tau\tau} &= \frac{\sigma_{qq}}{\sigma_{\tau\tau}} \quad = 26.3252 \pm 0.1635 \end{aligned} \tag{23}$$

From the literature[3], the expected quantity is R = 20.668 ± 0.032. But we have have obtained quite higher value for the electron channel and lower value for the tauons and muons channels. The expected sources of the errors are discussed in the section 7.

5.4 Breit-Wigner distribution

The cross-sections of the processes can be described by a Breit-Wigner distribution of the following form:

$$\begin{aligned} \sigma &= \frac{12\pi}{M_Z^2} \cdot \frac{s\Gamma_e\Gamma_f}{(s-M_Z^2)^2 + s^2\Gamma_Z^2/M_Z^2} \\ &= \frac{s\sigma_f^{peak}\Gamma_Z^2}{(s-M_Z^2)^2 + s^2\Gamma_Z^2/M_Z^2} \end{aligned} \tag{24}$$

where

$$\sigma_f^{peak} = \frac{12\pi\Gamma_e\Gamma_f}{M_Z^2\Gamma_Z^2} \tag{25}$$

Here, Γ describes the decay width of the corresponding particle. To verify this relation, we plot the cross-section of the different decay channels and the fit equation(24) given above. The fit results can be seen in Figure(16,17,18,19). The resulting fit parameter $\sigma^{Peak}, M_Z, \Gamma_Z$ and their errors can be found in Table 6.

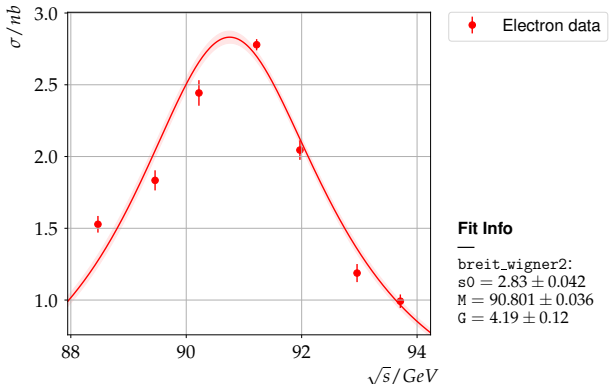

Figure 16: Cross-section for $Z^0 \to e^+e^-$

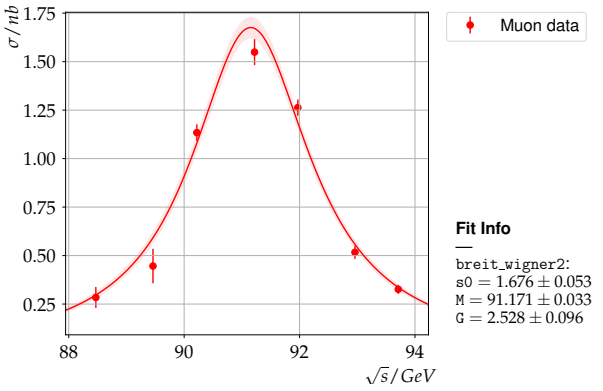

Figure 17: Cross-section for $Z^0 \to \mu^+\mu^-$

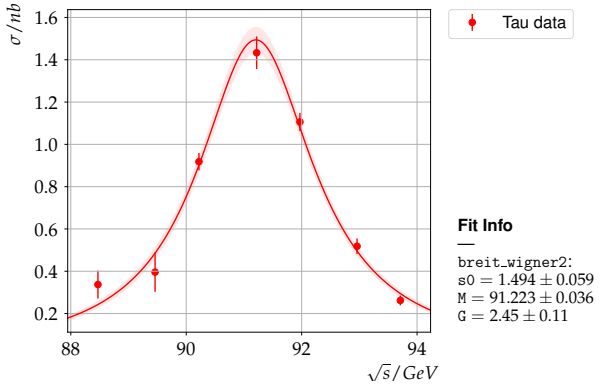

Figure 18: Cross-section for $Z^0 \to \tau^+\tau^-$

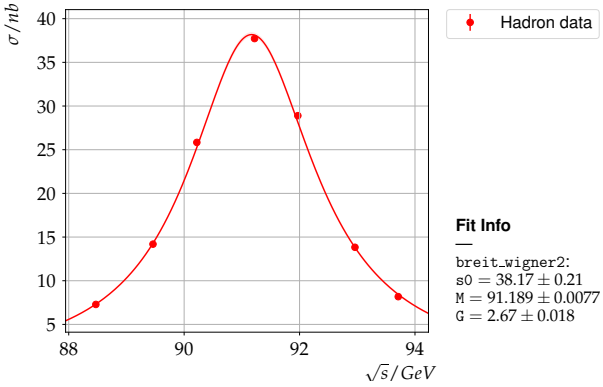

Figure 19: Cross-section for $Z^0 \to qq$

5.5 Goodness of fit

In Table6 two parameter which describe the quality of a fit are listed. The reduced chi squared χ^2 is the weighted sum of squared deviations per degree of freedom. In our case there are four degrees of freedom(number of data points – number of fit parameters).

In this variable one can assume, that the best fits are the one in which χ^2 is close to 1. Here, the fit for the muons and tau are close to 1. In other channels, there is large difference, which means that either the fit is not very good or the uncertainties have been underestimated.

The second variable is the p-value. In this case the muons and tau channel reach values of 0.013 and 0.162 respectively. The lowest p-value is reached in the elecctronic channel. It is safe to assume that the Breit-Wigner distribution is an idealisation of the real decay. Thus smaller errors lead to a deficient convergence of the fit algorithm.

The fit-parameters allows us to specify the mass of the Z-boson and its width. For that the mean of

	$\sigma_{peak}(nb)$	$M_Z(GeV)$	$\Gamma_Z(GeV)$	p-value	χ^2
e	2.83 ± 0.042	90.801 ± 0.36	4.19±0.12	0.000	11.7
μ	1.676 ± 0.53	91.171 ± 0.033	2.528±0.096	0.013	3.18
τ	1.494 ± 0.059	91.223 ± 0.036	2.45±0.11	0.162	1.64
qq	38.14 ± 0.21	91.187 ± 0.770	2.67±0.018	0.001	4.55
Mean		91.096± 0.2997	2.9595 ± 0.086		

Table 6: Fit parameters of the Breit-Wigner distribution. To quantify the quality of the fit, the p-value and the χ^2 is given.

M_Z and Γ_Z of all the channels are given in Table 6. From Figure 20 and 21, they show that the estimated parameter are strongly correlated. The associated literature values from reference[3]

$$M_Z = 91.188 \pm 0.002 \quad GeV \qquad \& \qquad \Gamma_Z = 2.495 \pm 0.002 \quad GeV$$

The fit parameters of $Z \to \tau^+\tau^-$ channel is accepted at the signifance of 5% where as for other decay channels, they are rejected at the significance of 5% according to the fit parameters[4].

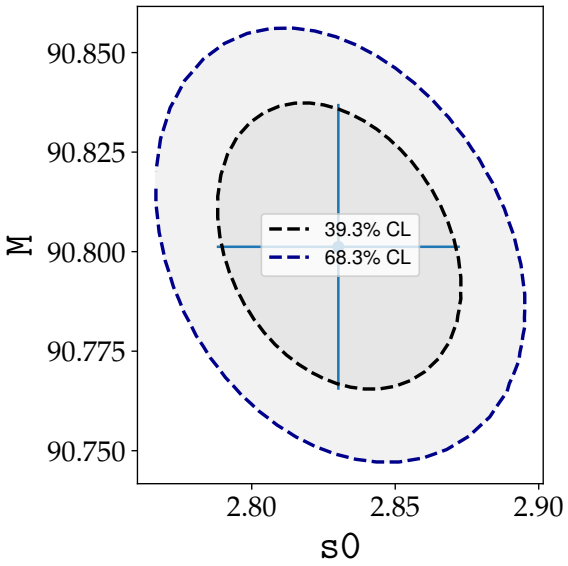

Figure 20: Contour plot of M_{Z^0} vs σ for $Z^0 \to e^+e^-$

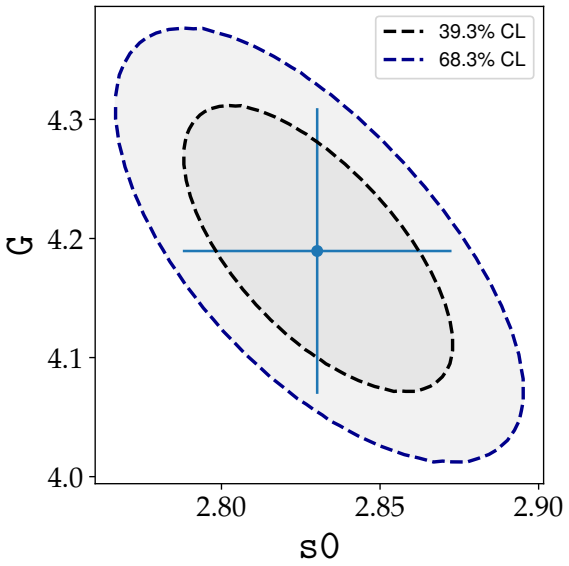

Figure 21: Contour plot of Γ_{Z^0} vs σ for $Z^0 \to e^+e^-$

5.6 Partial width of the channels

The cross-section at the resonance is given by

$$\sigma_f^{peak} = \frac{12\pi\Gamma_e\Gamma_f}{M_Z^2\Gamma_Z^2} \tag{26}$$

The partial width of the each channel is calculated using the equation (25). We get the result given in Table 7 and the error is estimated as

$$\frac{\Delta\Gamma_f}{\Gamma_f} + \frac{\Delta\Gamma_e}{\Gamma_e} = \frac{\Delta\sigma}{\sigma} + \frac{2.\Delta\Gamma_Z}{\Gamma_Z} + \frac{2.\Delta M_Z}{M_Z} \tag{27}$$

chanel	Γ_{cal}(GeV)	Γ_{lit}(GeV)
ee	117.49 ± 4.70	83.91 ± 0.12
$\mu\mu$	65.42 ± 28.34	83.99 ± 0.18
$\tau\tau$	60.58 ± 10.30	84.88 ± 0.22
hadrons	1594.99 ± 121.36	17.44 ± 2.00

Table 7: Partial width of the decay channels and literature value from reference[3].

The calculated values shown in the table 7, deviate a lot from their expected literature values. The main resaon of deviation is the weak estimation of the resonance cross-section and the decay with of the Z^0 boson.

5.7 Number of generations of light neutrinos

With the analysis done it is now possible to determine the number of neutrino families in the following way: The total decay width of the Z-boson can be written as the sum of the width of all decay channels,

$$\Gamma_Z = \Gamma_e + \Gamma_\mu + \Gamma_\tau + \Gamma_{had} + n_\nu \Gamma_\nu \tag{28}$$

Thus the error is estimated as

$$\Delta n = \frac{\Delta\Gamma^2_{Z^0} + \Delta\Gamma^2_e + \Delta\Gamma^2_\mu + \Delta\Gamma^2_\tau + \Delta\Gamma^2_{had}}{\Gamma^2_\nu} \tag{29}$$

This relation is valid if there are only the listed parts and the formula includes only contributions of neutrinos under the Z^0 -mass.The width of the neutrinos is $\Gamma_\nu = (166.33 \pm 0.50) MeV$[3]

In combination with the values from the Table (7), we obtain

$$n_\nu = 6.75 \pm 3.81$$

The values are much greater than the expected values with large uncertainities.

6 Conclusion

During the first part of the experiment, we got the satisfying results for the graphical analysis of some preselected data. However, in the second part of the experiment, our cuts didnot worked that well on the actual OPAL data since we got the results different from the literature values. We couldnot verify the lepton universality, the R value, the number of neutrinos. Nevertheless, we were able confirm the muon forward backward asymmetry parameter.

7 Discussion

During the analysis of OPAL data, all errors are based on the statistical fluctuations of the event number,i.e, $\Delta N = \sqrt{N}$. Nevertheless there are physical processes, which influence the uncertainty of the calculated constants and values systematically. Systematic uncertainities of the OPAL detector are unknown to us and a complete determination would be beyond the scope of this report.Aspects like the efficiencies of the different detectors and coverage of the solid angle are unknown and thus neglected.

In general the chosen cuts are not perfect. They are based on observations of the histograms, which can lead to errors. Ofcourse, the efficiency matrix should minimize the amount of incorrectly assigned events but the Monte-Carlo simulated data was only provided for one energy.Other points are the radiative corrections.

But based on the analysis of the observed number of events, for the 100% (theoretical) efficient cuts, we should expect nearly the same number of the events for the same integrated luminosity. But since the electron-channel cut is least efficient in our case, we should expect less number of events in the electron channel compared to others before applying efficiency matrix correction. But, in real, the number of observed events in the electron channel is too high despite inefficient cut which has lead to greater deviation from the values that are expected in the literature. Besides, from figure 20 and 21, they shows that estimated value cross-section (σ), mass of the Z-boson, (M_{Z^0}) and the decay with Γ_{Z^0} are correlated. So, wrong estimation of one parameter will lead to error in other parameters.

8 Acknowledgement

We wish to acknowledge Omer Ogul Oncel for his helpful guidelines and discussion during the course of the experiment.

References

[1] Retrieved from: "https://en.wikipedia.org/wiki/StandardModel"

[2] retrieved from "https://cds.cern.ch/record/2705419/plots"

[3] Advanced Lab Course manual, "E213: Analysis Of Z^0 Decays", Rheinische Friedrich-Wilhelms Universität Bonn, 2019

[4] Fitting: "http://www-ekp.physik.uni-karlsruhe.de/ quast/kafe/htmldoc/"

[5] M. Lefebvre1 et al: "Propagation of Errors for Matrix Inversion" , 2000

9 Pre-Lab Questions

9.1 Question1

$$\Gamma_f = \frac{N_c^f}{12\pi}\sqrt{2}G_f M_Z((g_V^f)^2 + (g_A^f)^2) \tag{30}$$

where

$$g_V^f = I_3^f - 2Q_f \sin^2\theta_W g_A^f = I_3^f \tag{31}$$

The following values are used:
$\sin\theta_W = 0.2312$
$M_Z = 91.182GeV$
$G_F = 1.1663 \times 10^{-5} GeV^{-2}$
$N_c^f = 3(quarks)$
$N_c^f = 3(leptons)$

The decay width for leptons:
I_3^f = -1/2
Q^f = -1
g_V^f = -0.0376
g_A^f = -1/2
Γ_f = 83.39MeV
Γ_f^{meas} = 83.8 MeV

The decay width for Neutrinos:
I_3^f = +1/2
Q^f = 0
g_V^f = +1/2
g_A^f = +1/2
Γ_f = 165.8MeV
Γ_f^{meas} = 167.6 MeV

The decay width for u and c Quarks:
I_3^f = +1/2
Q^f = +2/3
g_V^f = 0.1917
g_A^f = +1/2
Γ_f = 285.3MeV
Γ_f^{meas} = 299 MeV

The decay width for d,s,and b quarks:
I_3^f = -1/2
Q^f = -1/3
g_V^f = -0.03459
g_A^f = -1/2
Γ_f = 367.81MeV
Γ_f^{meas} = 378 MeV

9.2 Question2

The total Z^0 decay width is $\Gamma_{Z^0} = \Gamma_{hadrons} + \Gamma_{leptons}^{charged} + \Gamma_{leptons}^{invisible}$

where: $\Gamma_{hadrons} = 2 \times \Gamma_{up-tye} + 3 \times \Gamma_{down-type} = 1674.03MeV$
$\Gamma^{charged}_{leptons} = 3 \times \Gamma_l = 250.17MeV$
$\Gamma^{invisible}_{leptons} = 3 \times \Gamma_\nu = 497.4MeV$

Using the above values we get $\Gamma_{Z^0} = 2421.6MeV$

The cross-section is given by:

$$\sigma_f^{peak} = 6.448 \times 10^{-11} \Gamma_f GeV^{-2} \tag{32}$$

On calculating we get:
leptons : 2.09 nb
Neutrino : 4.16 nb
Up-type Quark : 7.16 nb
Down-type Quark : 9.23 nb

9.3 Question3

The change(in percentage) of the width of the Z^0 resonance curve can be calculated as $\frac{\Gamma_f}{\Gamma_{Z^0}} \times 100$
leptonic = $\frac{83.39}{2421.6} \times 100 = 3.44\%$
Neutrino = $\frac{165.8}{2421.6} \times 100 = 6.85\ \%$
Up-type quark = $\frac{285.3}{2421.6} \times 100 = 11.78\%$
down-type quark = $\frac{367.81}{2421.6} \times 100 = 15.19\%$

9.4 Question4

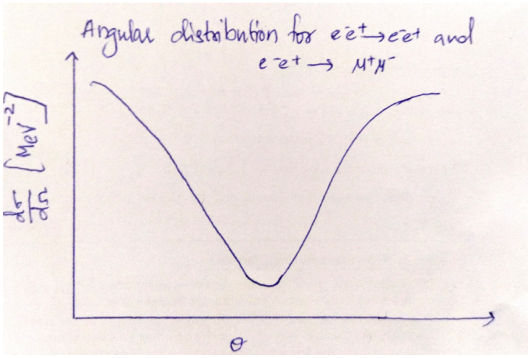

Figure 22: The angular dependence of electron and muon final states

The angular distributions for the $e^+e^- \to e^+e^-$ and $e^+e^- \to \mu^+\mu^-$are the same since it can be proven that the angular distribution is independent of the fermion flavor from the Figure(10) .

In the case of $e^+e^- \to e^+e^-$ we have two different contributions in the cross section, from the s-channel and the t-channel. The s-channel event produces a Z^0 particle while the t-channel is the elastic e^+e^- scattering(Bhabha scattering). The contributions to the cross section are separately drawn in Figure(11) .

9.5 Question 5

To calculate forward-backward asymmetry:

$$A_{FB} = \frac{3F_2(s)}{4F_1(s)} \tag{33}$$

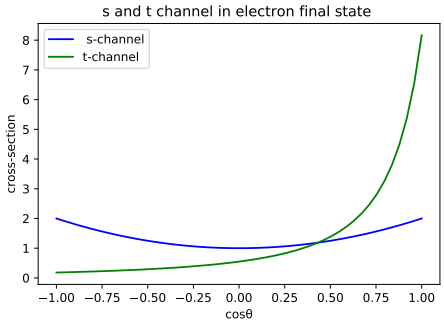

Figure 23: The angular dependence of of s and t channel in electron final states

where:
$F_1(s) = Q_f^2 - 2\nu_e\nu_f Q_f Re(\chi) + (\nu_e^2 + a_e^2)(\nu_f^2 + a_f^2)|\chi|^2$
$F_2(s) = -2a_e a_f Q_f Re(\chi) + 4\nu_e\nu_f a_e a_f |\chi|^2$
$\nu_f = \frac{I_3^f - 2Q_f \sin^2\theta_W}{2\sin\theta_W} = \frac{g_V^f}{2\sin\theta_W\cos\theta_W}$
$a_f = \frac{I_3^f}{2\sin\theta_W\cos\theta_W} = \frac{g_A^f}{2\sin\theta_W\cos\theta_W}$
$\chi(s) = \frac{s}{(s-M_Z^2)+\frac{is\Gamma_Z}{M_Z}}$

Center of mass energy(GeV) $\sqrt{s}$	A_{FB}		
	0.21	0.23	0.25
89.225	-0.1557	-0.1669	-0.1772
91.225	0.0199	0.0201	0.020
93.225	0.1834	0.1924	0.2041

Table 8: Forward-backward asymmetry of the muon decay channels.

10 Appendix

Events	Cltrk(N)	Ctrk(SumP)	Ecal(SumE)	Hcal(SumC)
1	2	50.9	82.6	0
2	2	91.9	90.0	0
3	3	82.5	92.3	0
4	2	80.9	86.8	0
5	2	38.1	89.5	0
6	2	83.8	87.5	0
7	2	87.4	93.2	0
8	2	69.3	90.7	0
9	2	96.1	98.4	0.5
10	2	90.3	90.6	0
11	2	92.1	88.5	0.5
12	3	81.7	91.6	0
13	2	89.6	92.5	0
14	2	61.1	89.2	0
15	3	88.4	89.1	0
16	2	90.9	90.5	0.3
17	2	64.6	88.8	0
18	2	95.6	96.2	0
19	2	93.0	90.8	0
20	2	94.1	89.2	0

Table 9: Measured parameters for $Z^0 \to e^+e^-$ channel

Events	Cltrk(N)	Ctrk(SumP)	Ecal(SumE)	Hcal(SumC)
1	2	90.1	1.6	7.0
2	2	93.0	1.6	8.7
3	3	96.8	2.0	0
4	2	89.1	2.3	8.5
5	2	90.5	1.5	7.2
6	2	91.8	1.8	4.3
7	2	86.3	3.7	3.3
8	2	99.2	1.3	2.9
9	2	88.2	1.6	3.0
10	2	90.9	1.3	6.7
11	2	95.6	2.5	6.1
12	2	75.3	3.1	6.8
13	2	85.2	5.8	4.4
14	2	98.6	3.6	5.7
15	2	86.8	1.9	7.9
16	2	98	1.9	2.0
17	2	108.3	2.0	8.5
18	2	92.4	3.6	6.7
19	2	92	1.9	22.6
20	2	92.6	3.6	5.7

Table 10: Measured parameters for $Z^0 \to \mu^+\mu^-$ channel

Events	Cltrk(N)	Ctrk(SumP)	Ecal(SumE)	Hcal(SumC)
1	15	37.7	37.0	14.1
2	17	39.2	66.8	9.9
3	46	64.6	53.0	13.0
4	36	45.3	53.2	7.7
5	41	59.9	53.2	13.8
6	9	21.9	65.2	8.8
7	16	55.9	50.4	24.3
8	30	38.1	68.3	1.8
9	22	34.4	75.5	6.2
10	36	51.2	62.3	5.5
11	23	63.1	56.0	17.2
12	23	59	60.6	8.5
13	26	62.2	67.2	20.4
14	30	43.3	1.7	4.3
15	40	47.8	61.4	5.7
16	19	67.9	52.1	10.6
17	14	52.1	61.0	4.4
18	29	82.6	53.8	16.4

Table 11: Measured parameters for $Z^0 \to \tau^+\tau^-$ channel

Events	Cltrk(N)	Ctrk(SumP)	Ecal(SumE)	Hcal(SumC)
1	5	74.0	51.1	10.2
2	2	46.5	17.3	8.2
3	2	30.	1.6	6.3
4	2	29.5	10.2	4.1
5	2	33.1	1.5	10.6
6	2	24.4	12.4	11.7
7	4	36.0	16.1	5.7
8	2	41.3	11.1	20.0
9	2	49.7	5.2	20.3
10	2	33.4	23.6	6.9
11	2	14.1	3.3	6.3
12	2	19.7	15.9	3.8
13	2	26.8	16.5	3.4
14	5	23.4	27	17.1
15	2	23.8	29.4	3.6
16	2	39	18.9	4.4
17	2	24.1	46.5	7.3
18	5	38.5	28.5	0
19	2	35.3	51.8	2.3
20	2	17.8	2.5	5.0

Table 12: Measured parameters for $Z^0 \to hadrons$ channel

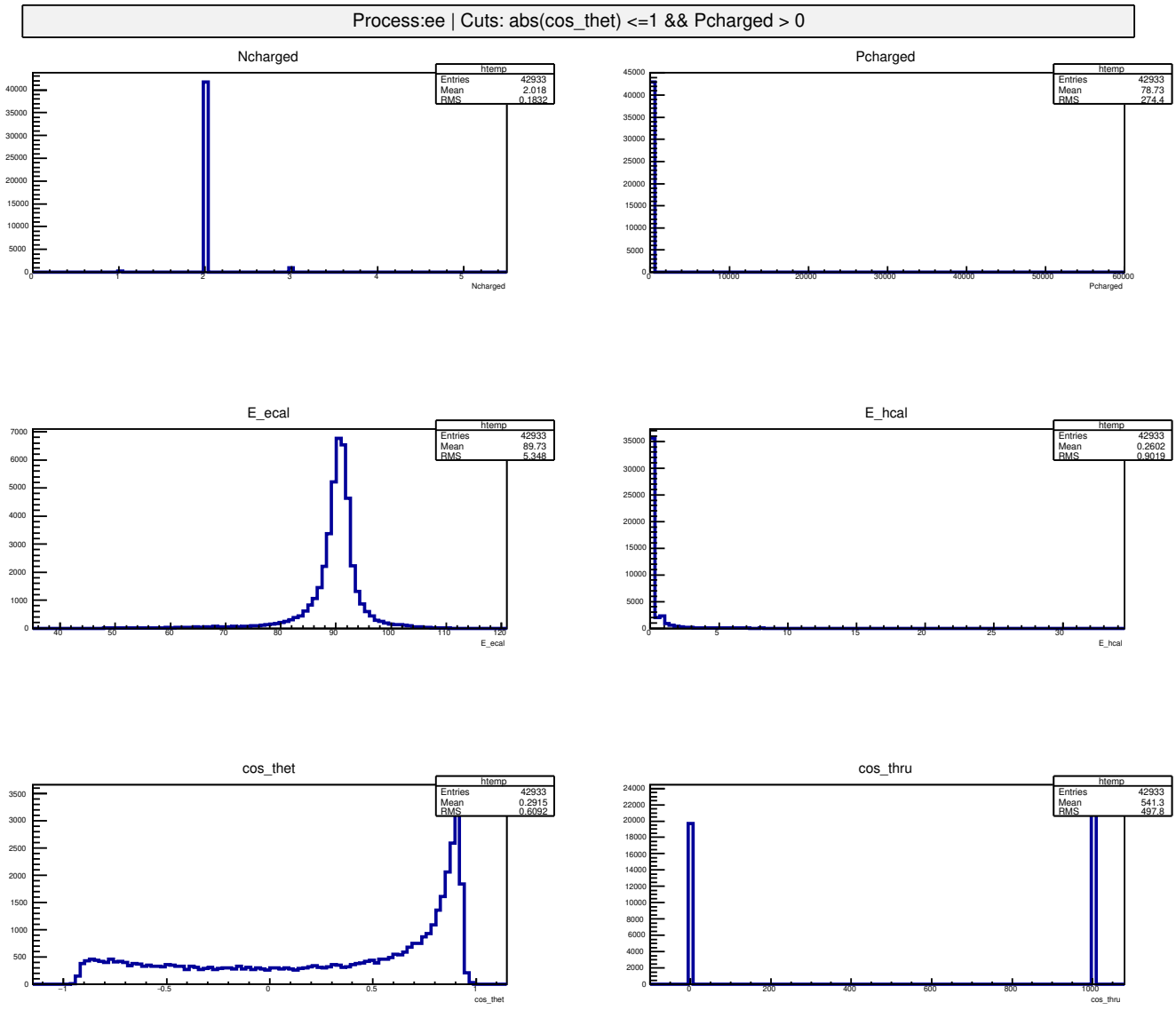

Figure 24: Plot of all the variable of the electrons channel

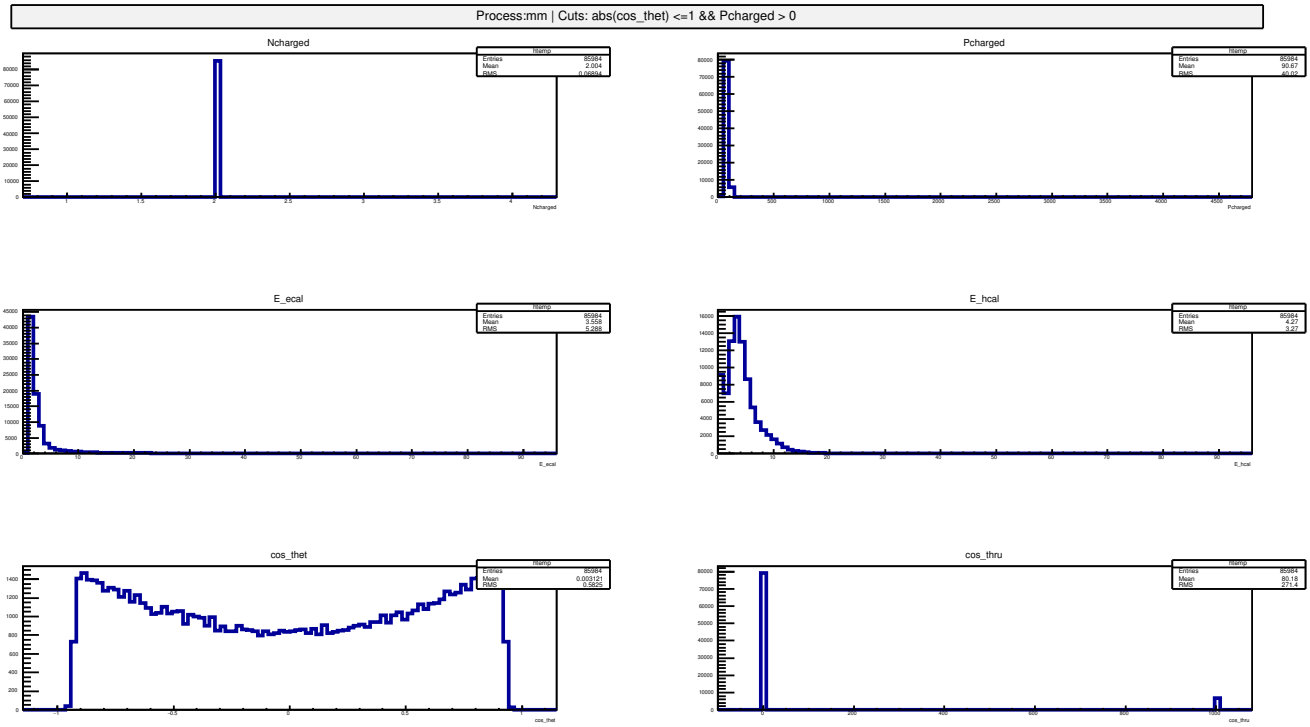

Figure 25: Plot of all the variable of the muons channel

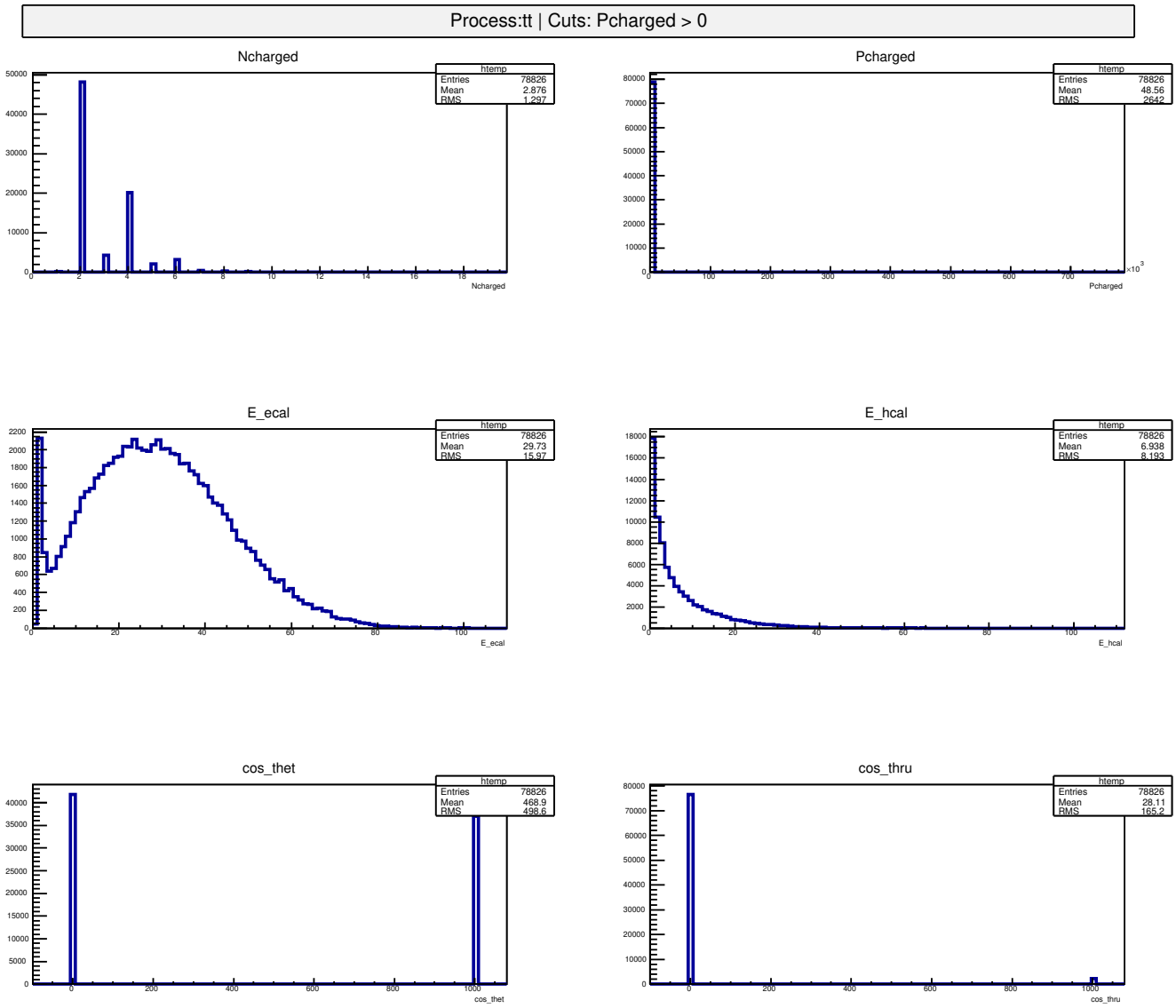

Figure 26: Plot of all the variable of the tauons channel

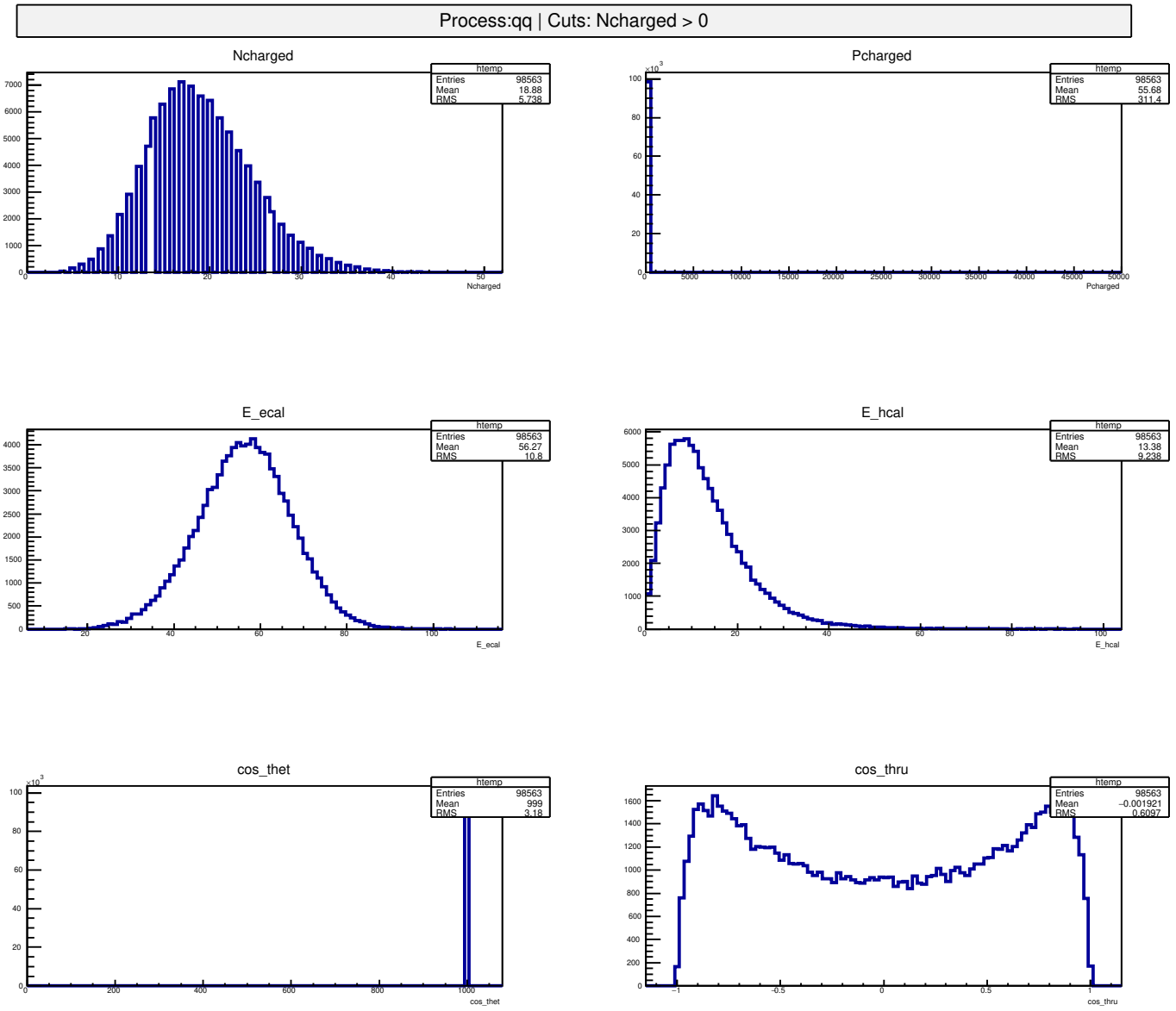

Figure 27: Plot of all the variable of the hadrons channel

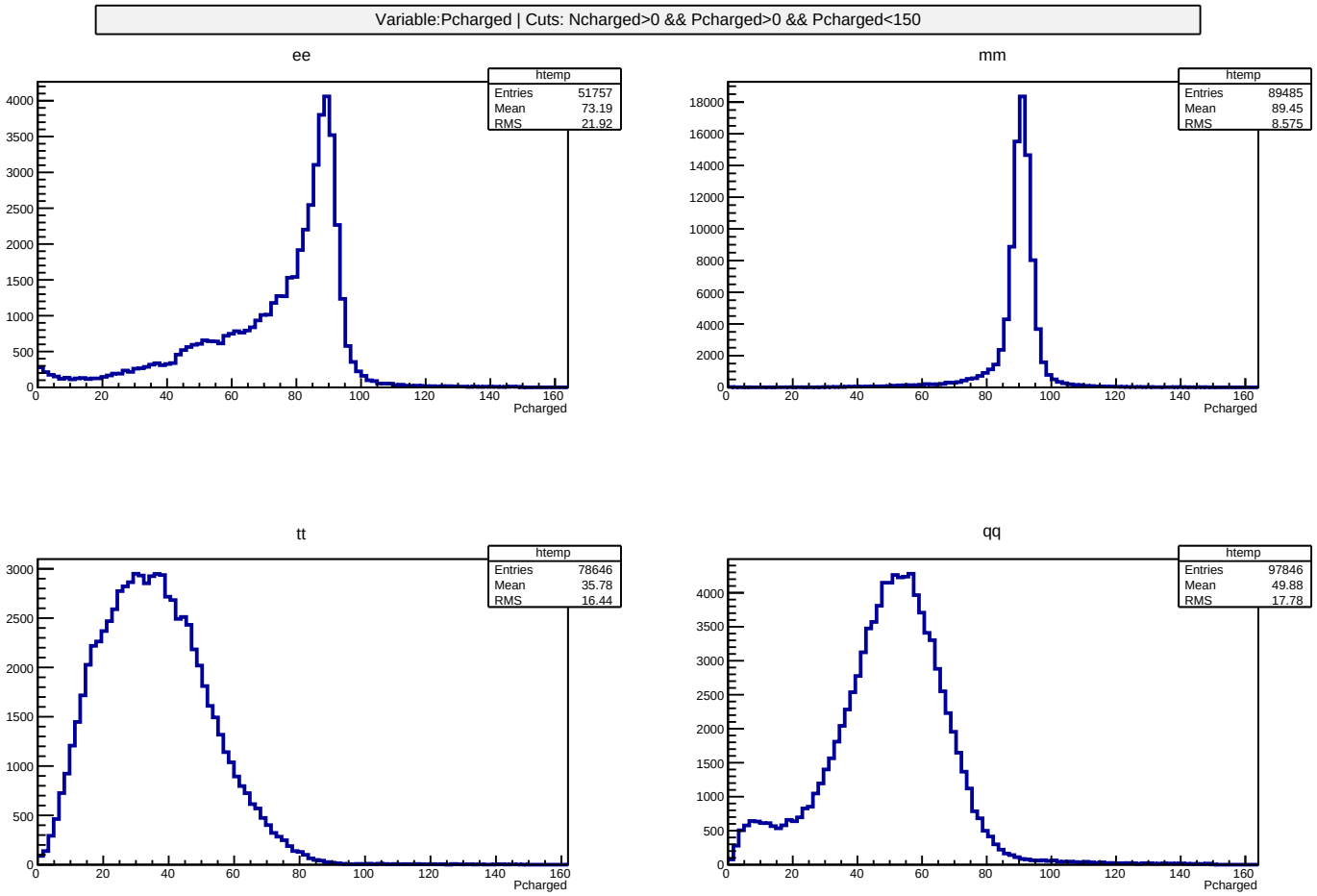

Figure 28: Plot of the Pcharged for all the sample to make the cut based on Pcharged

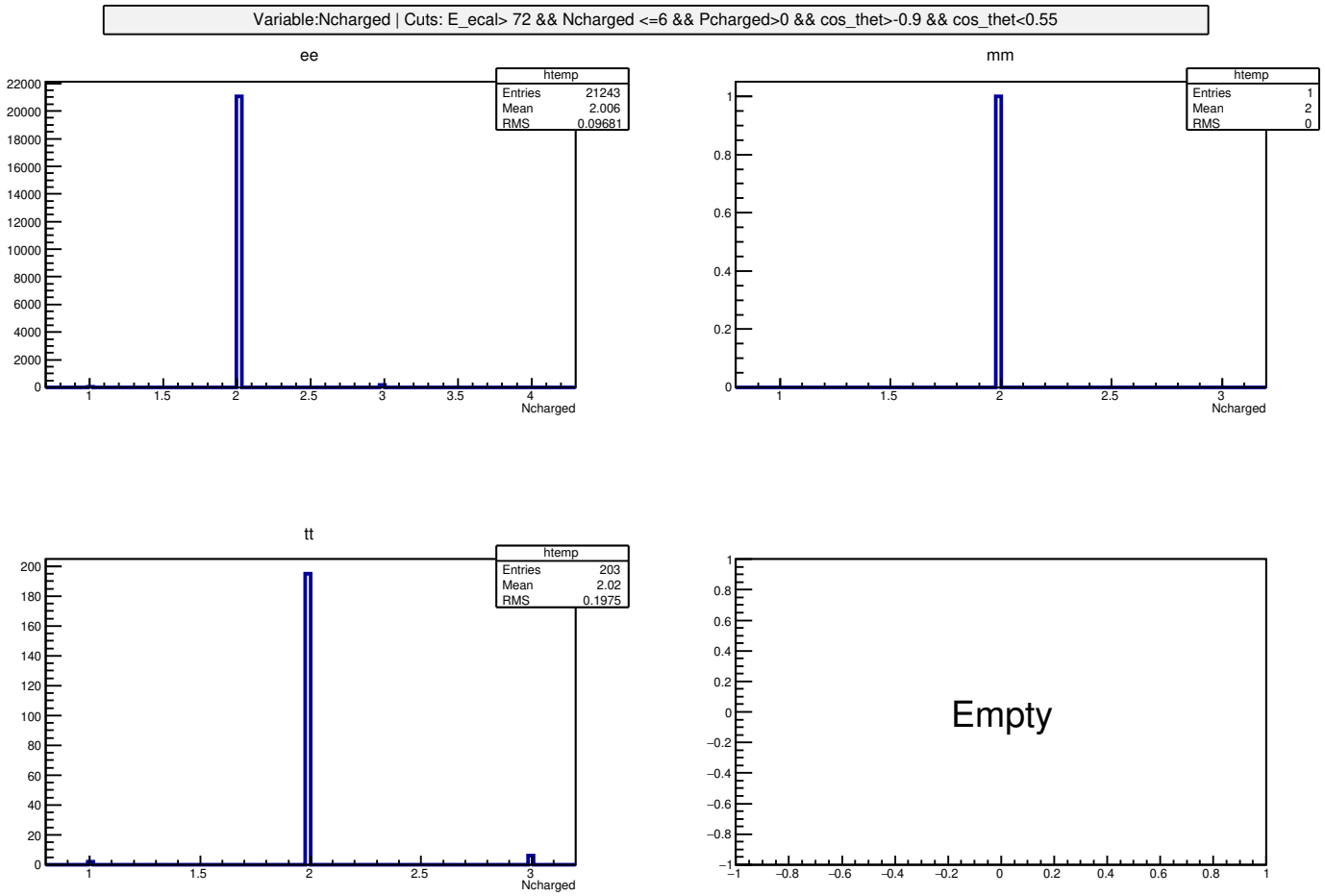

Figure 29: Cuts for e^+e^- channel

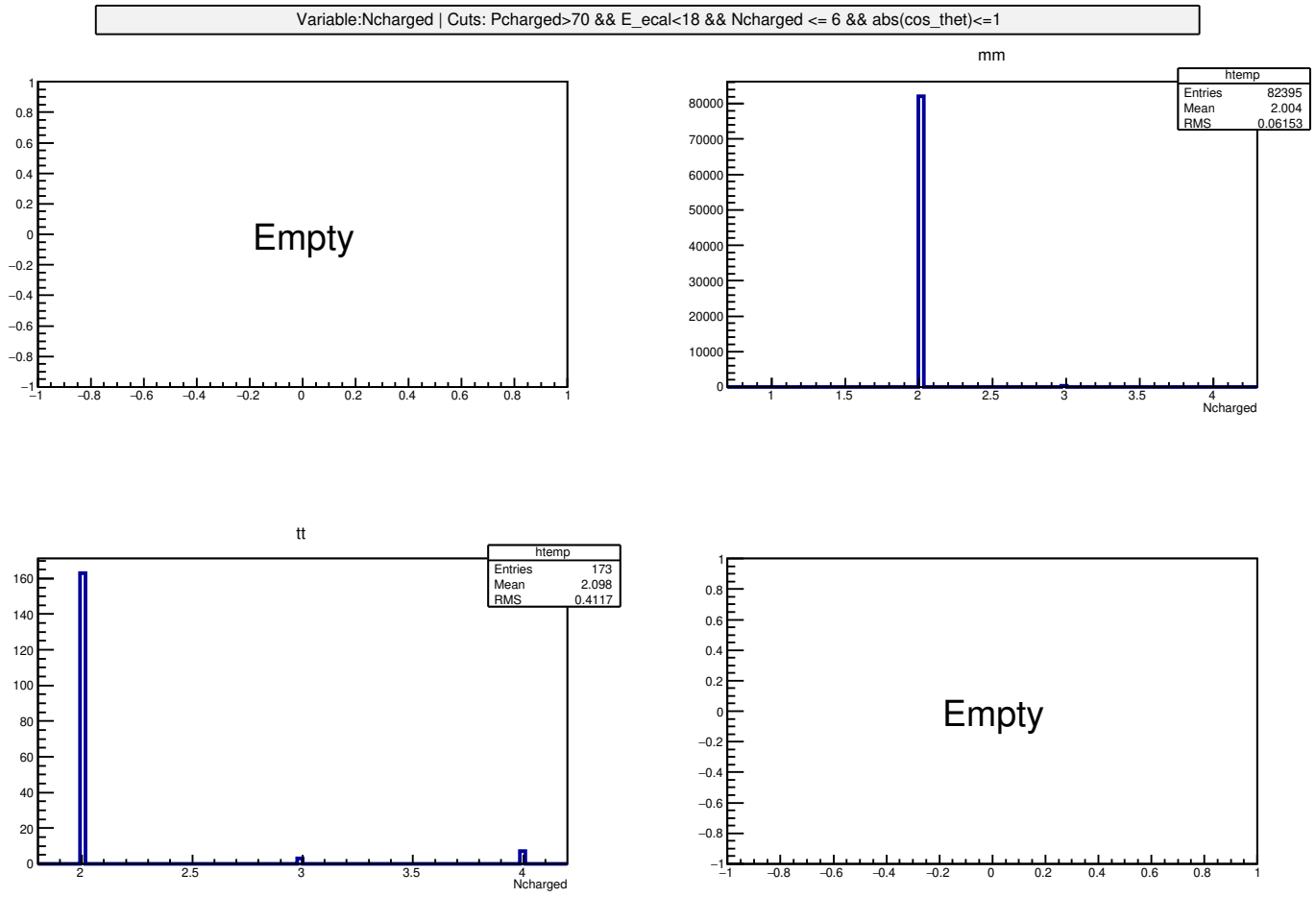

Figure 30: Cuts for $\mu^+\mu^-$ channel

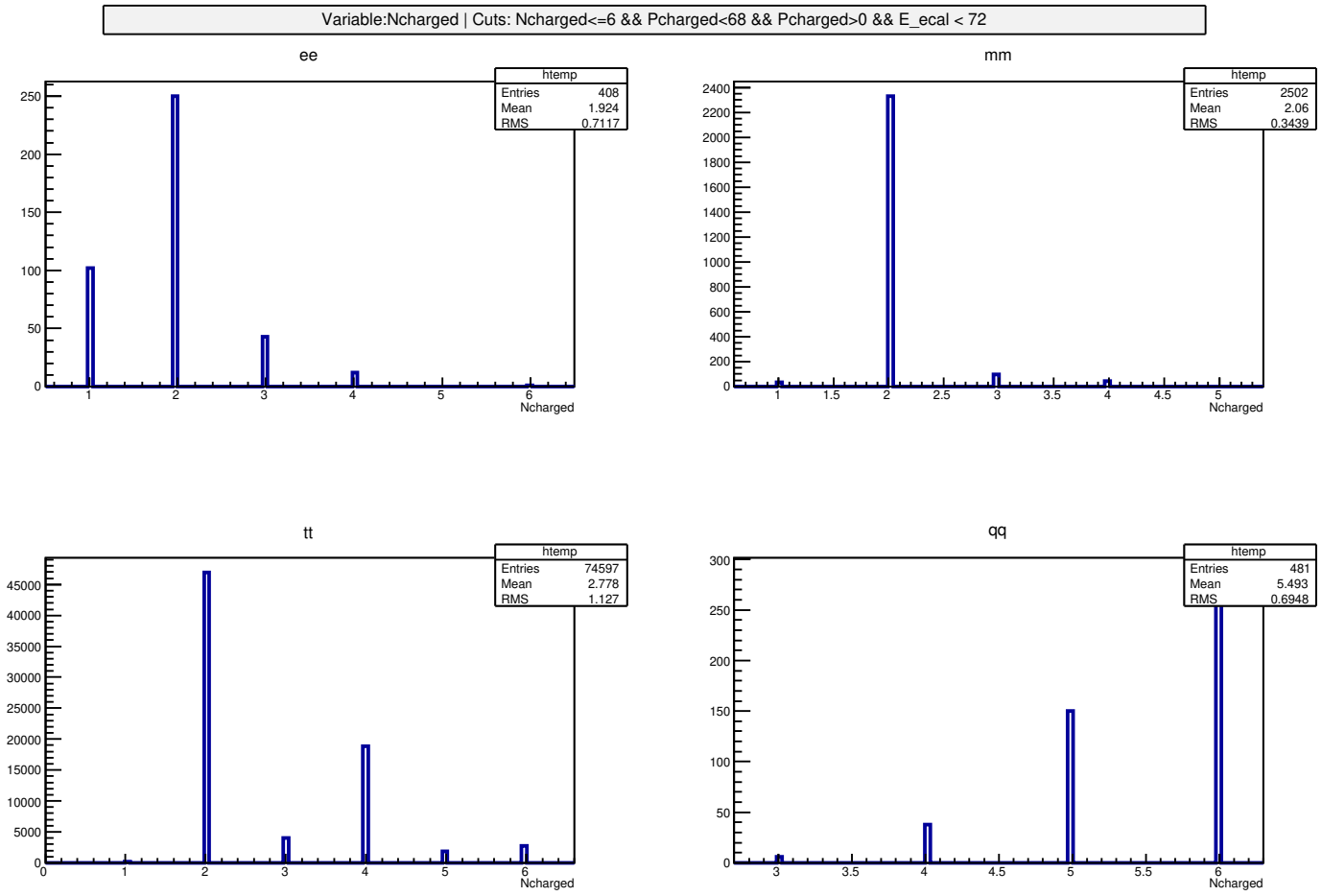

Figure 31: Cuts for $\tau^+\tau^-$ channel

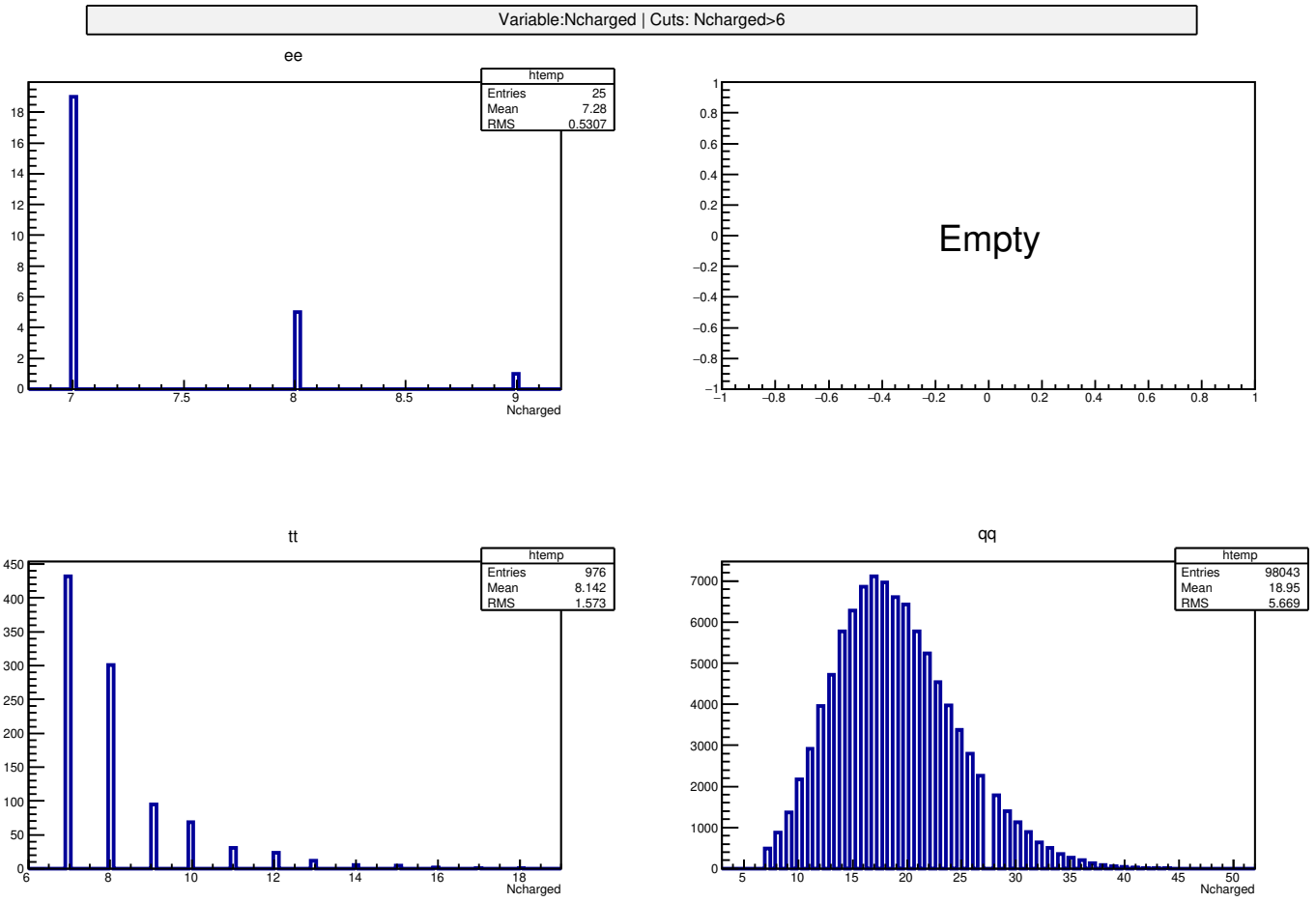

Figure 32: Cuts for qq channel